Designing an Optical Computer for three-dimensional cell-tracking

Imhotep Thomas Booth

Department of Physics, University of York

Submission Date: 04/2021

Designing an Optical Computer for three-dimensional cell-tracking

Contents

Designing an Optical Computer for three-dimensional cell-tracking

Abstract

The aim of this project is to improve methods for tracking fast-swimming bacteria in environmental or biomedical samples, to help identify species and quantify behavioural traits. This is performed using diffraction ring recognition based on holographic frame analysis by synthetically creating an archive of known diffraction images to be utilised in the Fourier domain by an optical computer, typically for three-dimensional tracking of microbes. The course of this work will involve looking specifically into the working details of optical components to allow us to simulate them digitally. Such that, system-implemented defects can be analysed to determine how best to design an optical computer to perform the above task. In so doing, we will show the comparative effectiveness of utilising the Structural Similarity Index (SSIM) and Mean Square Error (MSE) for feedback on how the optical computer is affected when the template archive is altered in attempts to improve the matching protocol. As well as how the greatest impact to the optical system arises with noise applied during the Fourier stage despite issues caused by Zernike polynomial patterns which occur on the synthetic templates. By doing so, our resulting optical computer design (The Hologram Analysis System 3 – THAS3) is capable of diffraction ring recognition corresponding to only 3 microns of depth error, and 1 micron of two-dimensional aerial error. Performing typically over 10,000 diffraction ring matches in approximately 2 minutes for a square array of 512 pixels width for the video frames being analysed.

Key Words: microscopic, holographic, tracking, optical, recognition

1. Introduction

1.1. The field of study

As Moore's law approaches its atomic limitation, digital devices will slow their rapid advancement requiring a new technology to take their place. A technology not limited by the electron interaction, such as that provided by photons in optical computation. Implementing photons and their superposition processes would overcome the atomic limitation proposed, opening a new avenue for future technological development.

Being able to design an optical computer is restricted by an understanding of the limitations of the components which constitute the system. Studying these limitations and breaking points would allow for the components to be adapted to overcome these boundaries and offer future growth in the area. Such boundaries are presented by components comprised of the Spatial Light Modulator (SLM), the Digital Micromirror Device (DMD) [1], and the Charge-Coupled Device (CCD) [2] which are distinctive components in any optical system.

A representative optical system such as the 4 focal-length correlator [3] is likely to consist of all the aforementioned components. A collimated light source such as a laser would project onto the DMD which would then cast an image towards the lenses, between which is situated the SLM which would perform a filtering effect in the Fourier domain [4], before finally the resulting filtered image is captured by the CCD [5]. While the process described for the 4F correlator is simple, the components involved are not. Since optical computing began in the 1980s, these components have advanced and undergone many adaptions in attempts to improve the overall system output. Only recently have these endeavours of advancement led to produce any notable outputs which could rival that of their digital counterpart.

1.2. Existing research

As previously explained, an optical correlator typically has an input signal from a Digital Micromirror Device (DMD) [6], which undergoes multiplication by some filter such as a Spatial Light Modulator (SLM) [7][8] in the Fourier domain. It reaches the Fourier domain by the theories of lenses and Fresnel Diffraction [9], showing the Fourier transform [10] of an image at the focal length **f** behind the lens when the image is length **f** in front of the lens. However, this only takes place with a coherent light source such as that from lasers due to complex amplitudes in the light.

This phenomenon has been previously used in 4F correlator research whereby the DMD is positioned a focal distance **f** from the first Fourier lens. The Fourier plane is then formed at a distance **f** after the lens which is where the SLM [11] is to be placed. There is a variety of different SLMs available ranging from reflective to transmissive and phase only SLMs [12] dependent on the operation required to be carried out. Continuing a further focal distance **f** from the Fourier plane, the second of the two Fourier lenses is placed to inverse Fourier Transform the manipulated (filtered) image back into a recognisable form. This image is formed at a distance **f** from the Fourier lens and received by a Charged-Couple Device (CCD) converting the photonic image

into a digital image for analysis. This totals 4 focal lengths from the starting input image to the ending output image, hence its common name the 4F Optical Correlator.

The components mentioned have previously been analysed in terms of the Structural Similarity Index (SSIM) [13][14]. There are several types of structural similarity algorithms in use such as Multi-scale SSIM, Percentage pooling SSIM, Complex-Wavelet SSIM, Gradient-based SSIM and Three-Component SSIM [15]. They all aim to advance the predictive accuracy of SSIM relative to human bias however they also increase the complexity of the computation. Along with SSIM, the Mean Square Error (MSE) is commonly used for its ability to directly compare two images as well as the Root Mean Square Error (RMSE).

A common example of processing used in 4F correlators is known as convolution [16] whereby the processing of information in the time domain is equivalent to point-wise multiplication in the frequency domain. Along with cross-correlation these make up the two most common uses of the correlator. With that being said, there is however little attempt made in previous research to take the next step in using the data presented by the SSIM and MSE values [17] to better design an optical computer to make use of the convolution or cross-correlation.

1.3. Project objectives

Given these previous areas of research, several particular complications can be seen which must be considered to answer questions which have not yet been researched. One of which is the issue of defects in an optical computer. In the 4F correlator there are various sections and components constituting the system, and with each new section another set of defects is allowed into the system. One such example of a defect is the DMD suffering from a pixel failure. Another major defect area is the lenses which perform the Fourier computation [18]. Here there are several places where noise can enter the system, both before and during the Fourier domain.

Along with defects which can enter the system are the actual details which are designed to be processed by the system. Specifically, the images being created by the DMD can be altered in several ways to impact how well the rest of the system can process them. Altering image contrast, sharpness, or brightness will be carried through the system and so obviously depending on what parameters are chosen here, the rest of the system is subject to perform accordingly.

Therefore, the project objectives are to decipher what effects the mentioned defects have on the system and to account for these in the design of the computer. As well as to decern what the best parameters are for the system to operate under to compute the necessary outputs. Such objectives can be accomplished using the SSIM and MSE analysis performed in previous research areas.

1.4. The course of the report

This report shall look at what issues are expected to be encountered during the investigation behind the problems so far brought to light. In so doing, an explicit research question can be arrived at. Furthermore, the physics principles which are necessary to answer the question will be formulated.

Apparent limitations to these theories will be sort for, regarding SSIM and MSE values. Following which the apparatus and steps of the methods will be presented including limitations of the said methods. Finally, results of the tests explained in the methods shall be given starting with experiments performed on the SLMs, followed by optical correlator analysis, finishing with tests regarding various defects possible in the optical system. Ultimately, arriving at logical conclusions drawn from these results. With the possibility of future adaptions to the experiments performed, as well as future research questions which would be of notable interest to be answered.

2. Methodology

2.1. Problems to be investigated.

Having arrived at the project objectives we will now proceed to uncover the anticipated problems to arise during the investigating of these objectives. In order to study noise defects entering the system a method of appropriate analysis must be fashioned. The use of SSIM and MSE values [19] are abundant in the course of image analysis. Therefore, the use of these values should overcome the problem exhibited here of a suitable method for image analysis. Given that this area of research has been dealt with vastly before, the problem of understanding results generated for these values is also consequently solved. In other words, a reliable control has been provided for evaluation between our created results and existing results already obtained on similar examinations. This ensures that all of our data can be understood not only correctly, but into its fullest connotations.

Following this are parameters employed into the optical computer which are devised to deliver the best possible results for the rest of the system. These parameters constitute the inputs to the DMD [20] and are the foundation of the processing. The challenge which arises here is after a number of operations have been completed on the original data, is it still possible to distinguish which operations correspond to the witnessed alterations on the output data. Essentially, how do we determine which component of the system design is responsible for a particular event observed at the output. The solution is (where possible) to perform the accumulation of modules in the system only after individual testing has been performed to establish how adjustments on the components affect their distinct outputs separately. In performing the method this way, it should enable us to better decipher the origins of the events seen and in turn, allow us to manipulate these events to our benefit. These origins would not be able to be differentiated in such an efficient fashion if an alternative method were performed in an attempt to locate influenceable events for our advantage.

2.2. The research question.

As seen in various previously conducted works, a major problem in optical computing is around the subject of components where defects enter the system and disturb the output of the computer beyond an acceptable amount. These defects can alter the processing steps in the system to the extent that the final output has been made so corrupted that it becomes inaccurate or nugatory. Therefore, in this project we will model the properties of optical components to determine how best to design an optical computer to overcome the impediments caused by defects in the system. With the end goal of achieving accurate data outputs with little loss along the chain of processing elements.

Answering this will provide a greater understanding of the studied components and allow the targeting of areas within components to be better aimed to evolve them. By studying specific breaking points at which the optical computer is suffering it should be possible to then focus efforts into developing ways to either counter the effects created or overcome them. In turn, evolving the components more effectively by targeting the weakest areas foremost, and by making better use of what already exists in the meantime to produce beneficial results.

Furthermore, taking a specific example for the purpose of an optical computer is likely to extend the effectiveness of this approach. For this project, the purpose of the optical computer is to be holographic microscopy analysis [21] in order to three-dimensionally track the entities in question which are archaea and bacteria. This is a typical use for an optical computer and a beneficial one given the number of additional innovations in bio-physics possible if improved equipment such as an efficient optical computer were provided for exploration in this field.

Overall, this study will contribute to the advancement of optical computer design to surpass their digital equivalent and overcome the technological impediment. This would lead to greater technological heights when optical computers inevitably overtake digital computers whose fate was set by the Moore's Law limitation.

2.3. Physics principles being utilised.

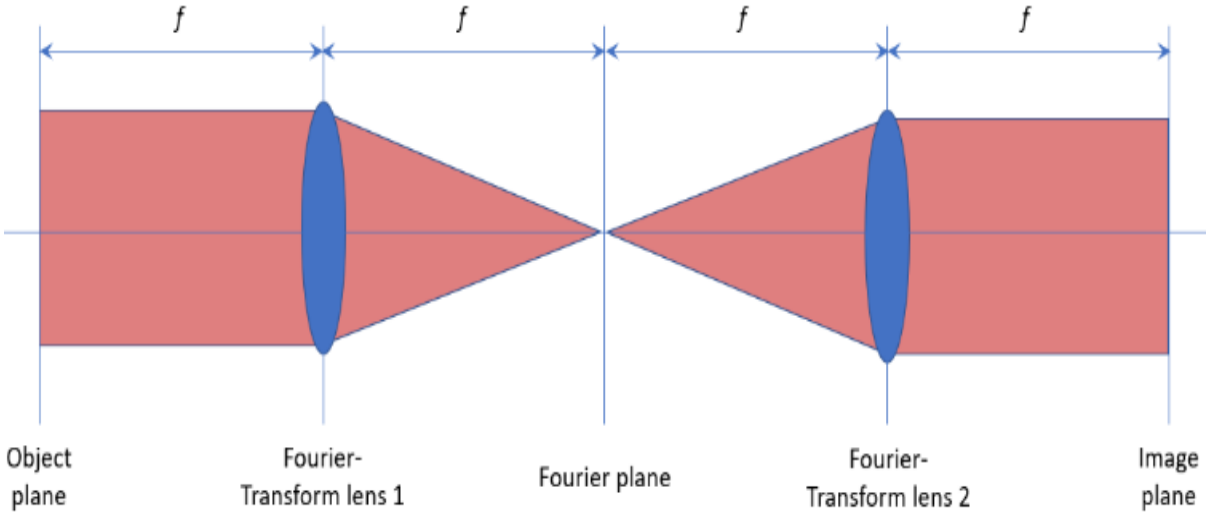

Figure 1: The 4F correlator demonstrating the location of the Fourier plane within the lens setup.

The physical basis for this project is the use of Fourier Transforms [22]. Simply, this is the transformation from a time dependant function into a frequency dependant function. This can be done using lenses such as in the aforementioned 4F correlator seen in Fig.1. The correlator makes use of this phenomenon whereby the Fourier plane, in which the Fourier Transforms are performed, is located in the centre of the pair of lenses. The mathematics required to perform such a transformation take a substantial period of time if calculated digitally [23]. However, due to the ability of the 4F correlator to create this Fourier plane, the 'calculation' performed by the correlator far surpasses the digital counterpart in terms of speed as this 'calculation' is literally performed at the speed of light. It then becomes evident, by exploiting this ability to our advantage we should be able to sufficiently improve optical computer technology up to and above the current level of digital technology, at least in terms of Fourier Transform architecture [24].

The principles regarding Fourier Transforms which are to be exploited are convolution and cross-correlation theorems in particular [25]. These theorems are amongst the most useful in terms of image recognition and manipulation which are required to answer the details of the research question. These theorems are presented below respectively in Equ.1 and Equ.2. They are also commonly used amongst various other research groups in this area thus stating their credibility for use here.

$$h(x) = \{f * g\}(x) = \int_{-\infty}^{\infty} f(y)g(x-y)dy$$

$$\hat{h}(\xi) = \hat{f}(\xi) \cdot \hat{g}(\xi)$$

*Equation 1: The convolution theorem $h(x)$ in which, f and g are integrable functions with Fourier Transforms $\hat{f}(\xi)$ and $\hat{g}(\xi)$ respectively, and $\hat{h}(\xi)$ is the Fourier Transform of the convolution. Where * is the convolution operation.*

$$h(x) = \{f \star g\}(x) = \int_{-\infty}^{\infty} \overline{f(y)} g(x+y) dy$$

$$\hat{h}(\xi) = \overline{\hat{f}(\xi)} \cdot \hat{g}(\xi)$$

Equation 2: The cross-correlation theorem $h(x)$ in which, f and g are integrable functions with Fourier Transforms $\hat{f}(\xi)$ and $\hat{g}(\xi)$ respectively, and $\hat{h}(\xi)$ is the Fourier Transform of the cross-correlation. Where $\star$ is the cross-correlation operation.

More precisely the method of matching a template image to its location in a source image is portrayed in Equ.3. This particular method of image recognition is known as a normalised correlation coefficient method.

$$R(x,y) = \frac{\sum_{x',y'}\left(T'(x',y') \cdot I'(x+x',y+y')\right)}{\sqrt{\sum_{x',y'} T'(x',y')^2 \cdot \sum_{x',y'} I'(x+x',y+y')^2}}$$

Equation 3: The matching function in which, I is the source image data, T is the template image data, R is the resulting matrix of the operations performed on these data sets which contain x and y pixel values.

Furthermore, the principles behind the Structural Similarity Index (SSIM) calculations required for analytical purposes are expressed in Equ.4. Here the equation contains three main parts, being that of luminance, contrast, and structure within any particular set of images to be compared.

$$[Luminance] \quad l(x,y) = \frac{2\mu_x\mu_y + C_1}{\mu_x^2 + \mu_y^2 + C_1}$$

$$[Contrast] \quad c(x,y) = \frac{2\sigma_x\sigma_y + C_2}{\sigma_x^2 + \sigma_y^2 + C_2}$$

$$[Structure] \quad s(x,y) = \frac{\sigma_{xy} + C_3}{\sigma_x\sigma_y + C_3}$$

$$SSIM(x,y) = [l(x,y)][c(x,y)][s(x,y)]$$

$$SSIM(x,y) = \frac{(2\mu_x\mu_y + C_1)(2\sigma_{xy} + C_2)}{(\mu_x^2 + \mu_y^2 + C_1)(\sigma_x^2 + \sigma_y^2 + C_2)}$$

Equation 4: The Structural Similarity Index (SSIM) function to be utilised during the course of this work, showing the luminance, contrast, and structure components in detail for clarity.

Finally, the Mean Square Error (MSE) calculations are performed pixel-wise in images using the equation shown in Equ.5. The pixel's value used for each pixel is the brightness taking on a value between 1 and 255 in grey-scale imaging.

$$\bar{X} = \frac{1}{n}\sum_{i=1}^{n}(X_i) \qquad MSE(\bar{X}) = E[(\bar{X} - \mu)^2]$$

Equation 5: The Mean Square Error (MSE) function to be utilised over the course of this work, showing the comparison between pixel values for computation. Where $\bar{x}$ is the expected value for the pixel in question, and μ is the true mean.

2.4. Limits to the theories

Limitations encountered with the SSIM tend to be with the image quality definition [26] as well as the natural image complexity problem. There is also the issue at the computational level involving the components of the SSIM, whereby the contrast and structural terms compute variance within the system which is very computationally demanding requiring most of the processing time [27]; Limiting the maximum possible array sizes able to be analysed [28]. There are however Faster SSIM algorithms being used at the expense of minimal accuracy [29]. In consideration to the image quality definition, although distortions may be clear visibly, they may not be so objectionably. Therefore, not equating visual error to that of quality loss when utilising the SSIM algorithms and so, the association between image fidelity and quality [30] is reasonable at best. Secondly, the complexity problem is how most psychophysical tests are carried out using simplistic patterns. However, these images are much simpler than that of any real-world image being tested with SSIM. Essentially the combination of many hundreds of more simplistic patterns leading to the question; can a model really compare two more complex patterns and generalise hundreds of simpler patterns to evaluate how these more complex images are correlated.

Other such limitations are encountered when using Mean Square Error to compare images [31]. When using the MSE to predict human perception in terms of image fidelity as well as image quality it becomes apparent that, dependent on the type of distortion upon images, the values of the MSE do not correspond to a visual human comparison of the same image distortions. Specifically, taking the rotational distortion of an image resulting in a drastic increase in the MSE value when visually the image is almost identical in quality. A property of MSE is that if the pixels within the image are reordered in the original image and the resulting image in the same manner the MSE value will remain unchanged. This can cause a severe perceived fidelity issue wherein the reordered resulting image can look much noisier than the original resulting image when white gaussian noise is added [32].

2.5. Apparatus being used.

In order to simulate the optical components, computational models must be created. These models will be formed using the well-known Python program along with supporting Python libraries. The images being used at all times in the course of this work will be kept to the same format for consistency. It was found the JPEG format performs a frequency-space compression on images. This is hazardous in terms of Fourier Transformations and can lead to anomalous results, and so instead the PNG format is used. In terms of video, the format is AVI as this format type is typically better quality than the MP4 format which is another typical video format commonly used.

Concerning the Python libraries, a wide variety were drawn from not only for their unique abilities but for their previous usage by numerous other researchers. These are namely: Mayavi [33] for three-dimensional analysis and presentation, OpenCV [34] for image manipulation and analysis, Holopy [35] for a multitude of diffraction ring analysis, and PyQt5 [36] for the user interface incorporated into The Hologram

Analysis System as well as the combination of all the previous modules into a singular application.

In conjunction with these libraries, which are dedicated to image analysis and presentation, are the libraries responsible for the more fundamental processing within the coding. Such libraries as NumPy which extends the Python abilities in terms of array usage and has been an open software for public practice since 1995. Having well-developed software sets up the remainder of the simulations to also run smoothly.

2.6. Methods of study

Commencing with the optical components to be simulated. A main component to be created is the Spatial Light Modulator (SLM) for which there are a variety of different options to be examined. These range from Low pass to High pass filters with distinctions of Ideal, Butterworth, and Gaussian being standard options. Here pixel values from the input image to the filter get multiplied by the particular mask function which is operating on it such that the output image is the convolution of the two. Moving to the lenses, they are simply a mathematical calculation of the Fourier Transform. Throughout the simulation, lenses are to be used in pairs at distances of exactly a focal length away from the next component. This means entering and leaving any particular lens is just the Fourier or inverse Fourier Transform of the image array entering or leaving the lens setup, respectively.

The combination of the previously simulated modules creates the 4F correlator. The method of doing this involves five stages. The input stage, simulating the DMD, which is the conversion of the image itself into the array data to be used for processing throughout the rest of the system performed by the OpenCV library. The first of the two lenses which takes the array data and performs a Fourier Transformation to it followed by shifting the zero-frequency component of the Fourier signal towards the centre of the image. The third stage is the SLM filter being applied to this centred-Fourier signal by multiplying the two arrays. The fourth stage is the second of the two lenses which performs the inverse Fourier Transform to the filtered-centred-Fourier signal by decentralising the zero-component while preserving the phase of the signal then applying the mathematical inverse function. This culminates to the final stage where the array can be outputted as an image by OpenCV much like a CCD capturing image data.

The subsequent methods are implementation of noise into the system. As stated before, there are various points of entry for noise into the system and here, we will look at three stages. The first is the implementation of noise onto an image before it enters the lenses of the 4F correlator. The second is the implementation of noise in the Fourier plane. And the third is a different form of ‘noise’ or rather defect on the DMD to represent a pixel breakdown such as a faulty mirror. The noise itself is known as white gaussian noise and is formed by creating a random distribution of values less than 0.1 which are then subtracted from the pixel values corresponding to the respective positions in the original image which noise is being convoluted with. This leaves an output image with a slightly ‘fuzzy’, whiter appearance. For the third ‘noise’

defect, small black squares are positioned onto the original image to simulate pixel failures.

The aforementioned SSIM and MSE values were taken and performed by using the library ‘skimage’ which conveniently provides the SSIM function. This must be applied to two arrays which are of the same dimensions. Likewise, the MSE function is also from the same library and is applied to two images by subtracting the array of one from the other, squaring those values and finding the mean of that array for creditable image quality assessment [37].

Moving to holographic analysis [38] and the application of holopy for the first time arises. Initially this will be used for 2D analysis as well as creating synthetic diffraction ring patterns. For 2D analysis, the raw image, and the background image (without the sample forming the hologram) are input into holopy along with the data concerning the laser, the CCD pixel spacing, and the refractive index for the sample medium. This is then utilised by holopy to produce a chosen number of reconstructed images at depth intervals which must be chosen to be a multiple of the laser wavelength so as to correct for complex superposition irregularities in the produced slices. For the creation of synthetic templates, the position and dimensions of the synthetic microbe are set, along with previous experimental parameters of laser wavelength, CCD spacing, and sample refractive index. Finally, the CCD capture dimensions are set, and synthetic diffraction ring templates can be generated. While holopy was designed to create 2D slices of a volume, this was redesigned to form the entire 3D volume for display and comparison purposes. This was done using the Mayavi library by compiling these slice arrays using specific MArray formats and reducing the RGB readings taken down to a single averaged array for these 3 colours. Finally, the Mayavi parameters required are to visualise only intensities in the 3D plot above a chosen threshold value to show the approximate positions of the microbes with a fringe surrounding them, this can also be enhanced by using the contour function to better show the anticipated outlines for the bacteria overlayed on the intensity plot.

Finally, the culmination of all the previous tests leads to the first stages of production for The Hologram Analysis System (THAS). Using the 4F correlator system with a matching filter applied for the SLM in order to attempt to match template images created by holopy to the source image being that of the holographic image; using Equ.3. Essentially, attempting to recognise a diffraction pattern on the original image without having to use the Rayleigh or Mie reconstruction routines. Different depths are then attempted to be matched from an extensive archive leading to the third dimension being found without the use of reconstruction routines. There is a threshold value to cut off matches which are not adequate, and the aim is to attempt to increase this threshold value as much as possible while preserving the number of correct matches as much as possible. We must also ensure the matches being found are not skewed over multiple different depths as this drastically impacts depth placement error.

2.7. Limits to the methods

The OpenCV library which converts images into data arrays has some discrepancies regarding RGB and BGR conversion types producing slightly different outputs despite the same image being processed. This is a method limitation seen as the theory says it should be identical but the use of OpenCV has constituted slight variations. The holopy parameters have to be set such that specific depth intervals are taken for the slices to reduce complex superposition issues. This limits choices of what would have been useful data for depths. Secondly, holopy forms a 'fringe' pattern which should not be there theoretically. It limits the quality and size of the templates able to be collected. The theory suggests perfect alignment for each of the individual components which would not actually be true if these simulations were constructed in reality and so limits how accurate the simulation actually is. This includes thermal fluctuations in the cameras for example which would lead to additional errors in positional analysis which have not been incorporated into these methods. With all that being stated however, the methods chosen are anticipated to still be appropriate to address the research question.

3. Results and Discussion

3.1. Spatial Light Modulators

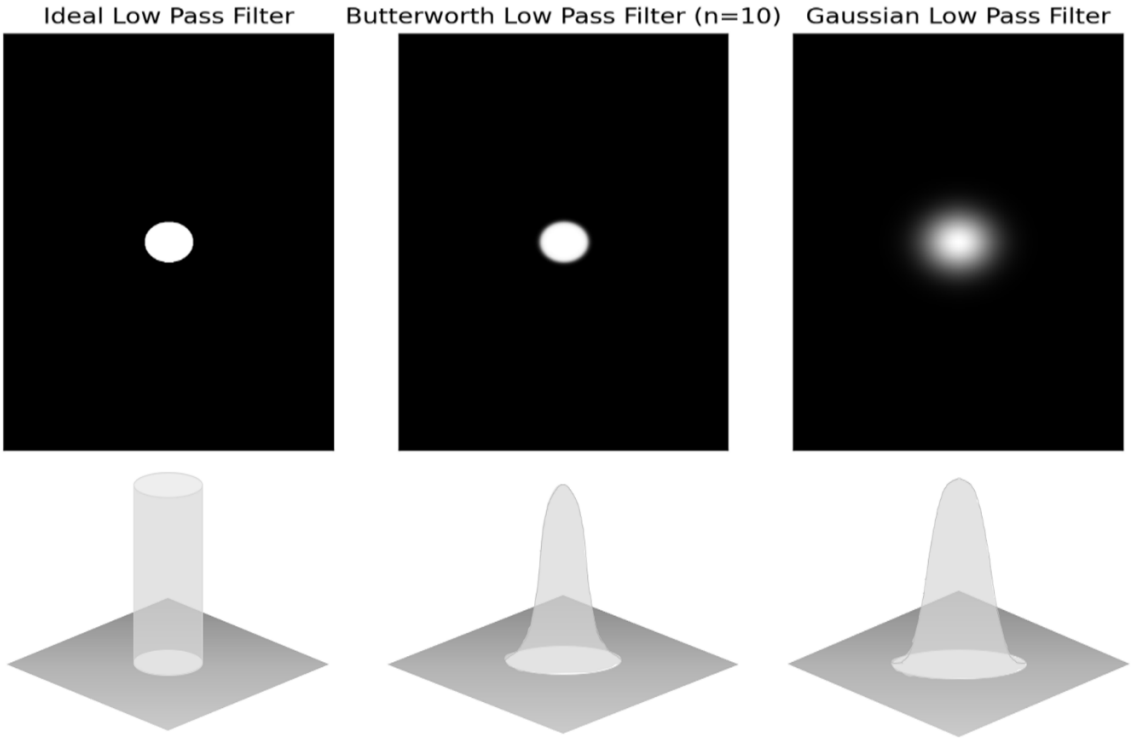

Figure 2: The Ideal, Butterworth, and Gaussian Low Pass Filters in 2D and approximate 3D representations.

Above in Fig.2 are the results of simulating the variety of filters previously mentioned. Each filter type is presented with its 2D perspective as well as the approximate Point Spread Function (PSF) in 3D below it. As expected, the results here show a solid and reliable foundation from which the rest of the project is to build on.

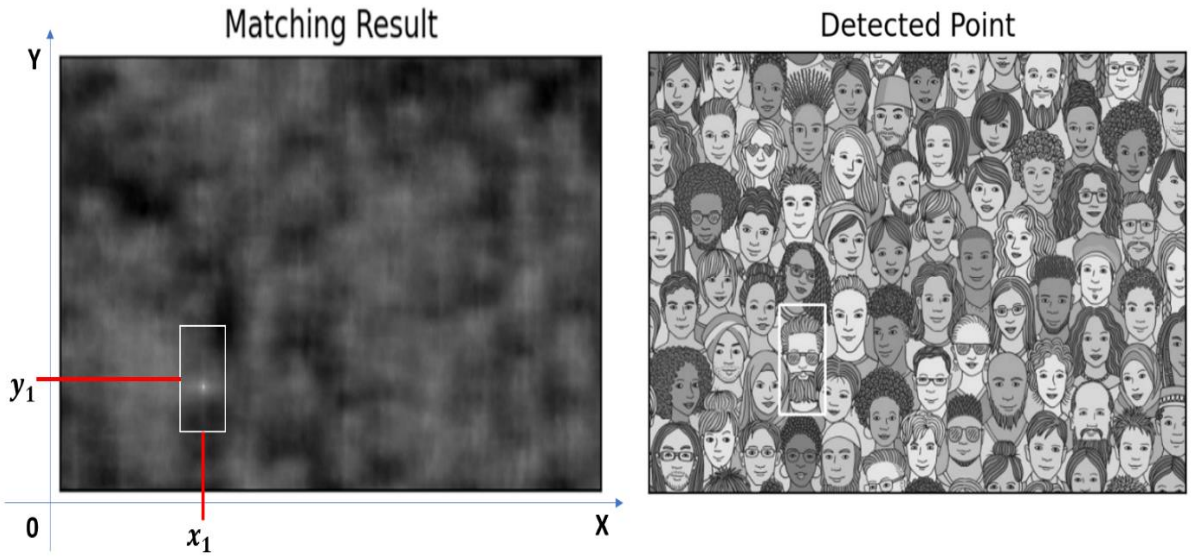

Figure 3: The Matching Filter simulation showing on the left the resulting output of the system, and the right the overlayed results of the system for clarity that the result is indeed correct.

Along with the mask testing is the match filter testing results which are SLM based results. This is shown in Fig.3 where a typical crowd picture is used as the source image, and the located man possessing a beard and sunglasses was the template image attempting to be recognised from the source. On the right is the rectangular box overlayed on the source image for clarity, which is centred on where the template core is computed to be found. On the left is the actual output from the simulation where a significantly bright singular spot can be seen at (x_1, y_1). This high intensity point is the identifying feature in the Matching Result image showing where constructive superposition has occurred to a magnitude larger than any other point in the image. It is the coordinates found which are the final output of this module as they indicate the 2D location of the template. It can also be seen that the bright PSF covers a range of a few pixels. This range is the error for the 2D positioning and it is notably small here forming only a single-pixel-radius circle in whose area the true centre is predicted to be located.

Several such templates were tested, all producing likewise accurate results signifying this matching filter simulation performs well to within a pixel error for 2D location. In terms of the research question, here we have successfully modelled the properties of the optical component known as the SLM. And through repeated testing, found the results of the above matching filter, which follows the function indicated in Equ.3, to perform admirably.

3.2. Optical Correlators

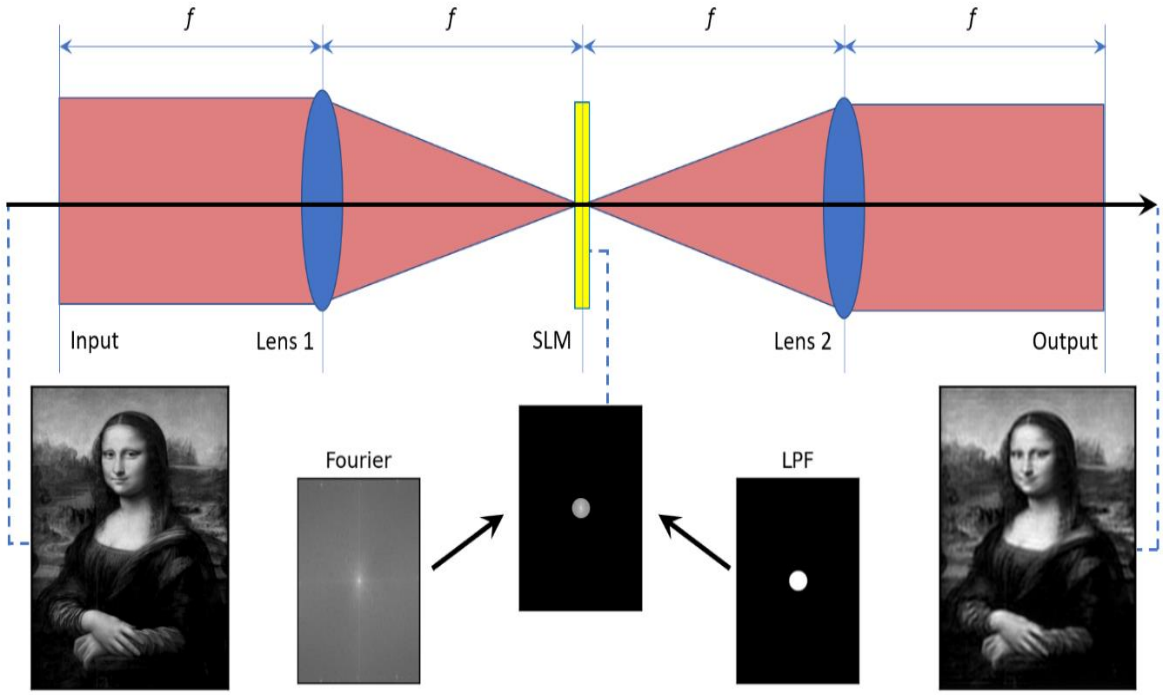

Figure 4: The 4F correlator setup containing the Ideal Low Pass Filter (LPF) for the SLM mask, with the famous Mona Lisa as the Input image, resulting in a degraded Output image of the Mona Lisa.

Previously the 4F correlator was portrayed, and here it has been fully simulated by the Python code to apply a mask to an image such as the Mona Lisa as depicted in Fig.4. It is evident that the Output image has been degraded in terms of image quality as is to be expected when using the ideal LPF as this filter removes the finer definition of an image which is contained in the higher frequency components. Therefore, as it can easily be seen the simulation is consistent with what was to be expected, it can be said the module works flawlessly. The central section of the figure depicts the inner workings of the correlator by combining the filter with the Fourier plane to visualise what is actually taking place.

While this simulation works well, the question of the Modulation Transfer Function (MTF) of the system is highlighted. Now for the first time there are several components accumulating to form a single module each with their own MTF properties which also combine to form a full MTF for the module as a whole. In various previous works, the MTF has been examined and is clearly a useful tool for any optical engineer to choose components such that they draw out the best from a particular system. And so, given the already extensive knowledge of this area, it can be assumed that when the particular components are chosen to form this correlator in reality, that the rules of the previously examined MTF are applied [39] and need not be touched upon here.

3.3. Equipment defects

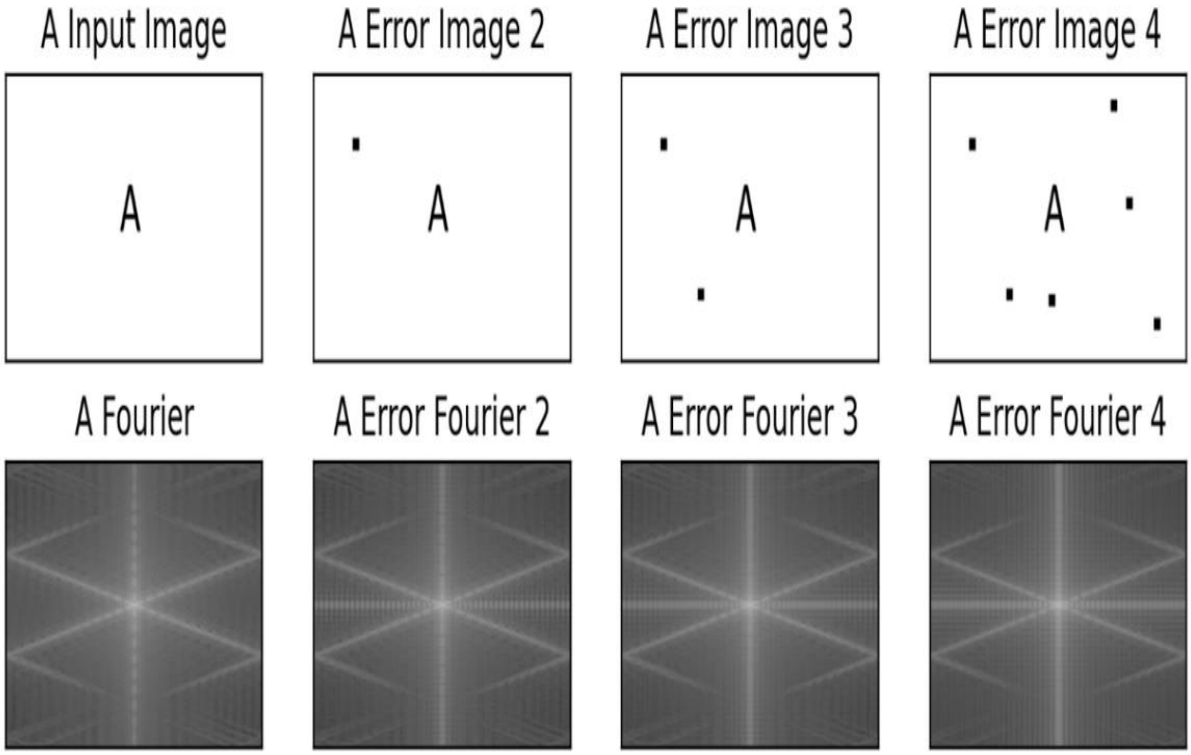

Figure 5: The multiple pixel failures on the DMD, shown by the black squares above, and the corresponding Fourier domains outputted, below in each case, for comparison as the pixel defects increase in magnitude.

In terms of equipment defects, the only component analysed was the Digital Micromirror Device (DMD). Given it is the founding component from which all other process run off, a good foundation is deemed necessary to better ensure good results later down the processing line. A possible defect in terms of DMD components is a pixel failure in the mirror array, leading to a faulty output in a small section of the whole array which has been indicated by a black square in Fig.5.

From the figure it can be seen that the A Error Fourier 2 image has a slight alteration from the original A Fourier image which is clearly due to the single pixel failure. The deviation is a plus-like pattern overlayed on the original Fourier image formed from the A input image. Continuing to the A Error Image 3 and 4 and their respective Fourier outputs, there is no significant additional variations from the single pixel failure seen in A Error Fourier 2. This suggests that no matter how many pixel failures are encountered (before it becomes obvious the DMD component is severely malfunctioning), that the same Fourier domain will be shown with the plus pattern representing the pixel failure. This can then be sort for by the computer such that if it occurs then it notifies the user a component failure has occurred.

In terms of the research question, the impediments caused by pixel failures within the system appear to have very minimalistic effects on the overall state of the system. Therefore, having seen these results it becomes apparent that these defects require very little effort to be accounted for, and so can be overlooked for the remainder of this project; with the awareness that if such a defect occurs, it can be detected and eliminated efficiently.

3.4. Noise defects

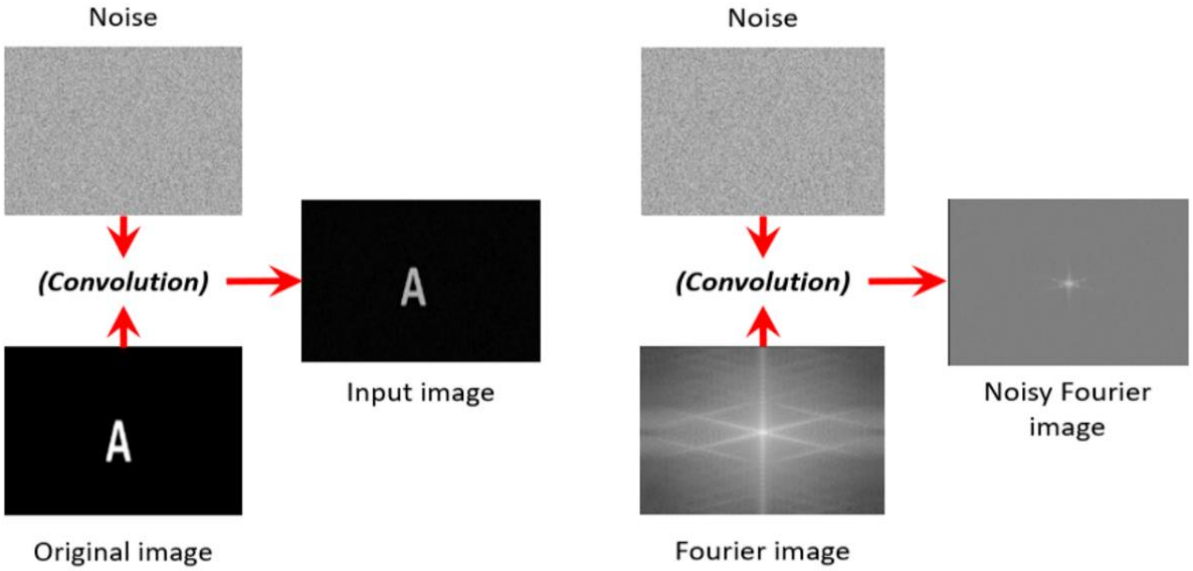

Figure 6: The combination of white noise with the various stages of the 4F correlator.

The results of noise defects occur in 2 stages. The first is noise defects entering the system before the lenses, and the second is after the first lens (during the Fourier domain). In both cases the same white noise has been employed and combined as seen in Fig.6. This shows the 2 cases in question, on the left being the noise applied before the lenses, and on the right being the noise during the Fourier domain.

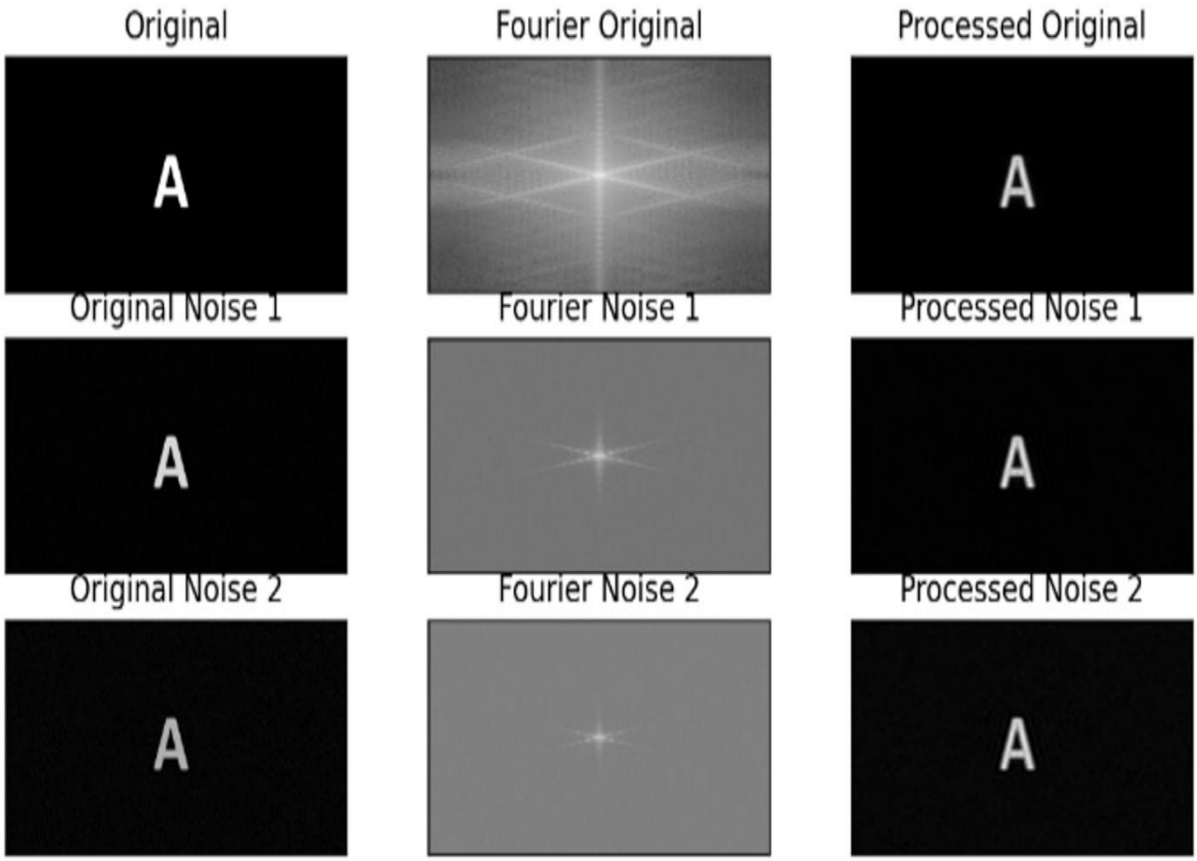

Figure 7: The effects of white noise being implemented on the original image for both the Fourier domain and the Output image (Processed image), for three different noise levels.

More specifically, each of the mentioned cases of defects were explored for 3 different noise levels to draw a comparison with escalating levels of noise entering the arrangement. Seen in Fig.7 are the results for said noise levels for the defect entering prior to the Fourier domain. The noise effects the original image which in turn disturbs the Fourier domain to result in an altered processed image. Looking at the three noise levels, it is evident that this is true for the original images as the A symbol appears notably darker, and the surrounding black section begins to exhibit white specks. As this arrives in the Fourier domain, it appears that the recognisable pattern from the Fourier Original becomes increasingly shrunk from the outer edges. This is akin to the effect of applying a form of Low Pass Filter whereby the central lower frequencies are passed through unaffected compared to the higher outer frequencies which become altered. The resulting processed image for each of the noise levels appears almost identical to the respective original input image.

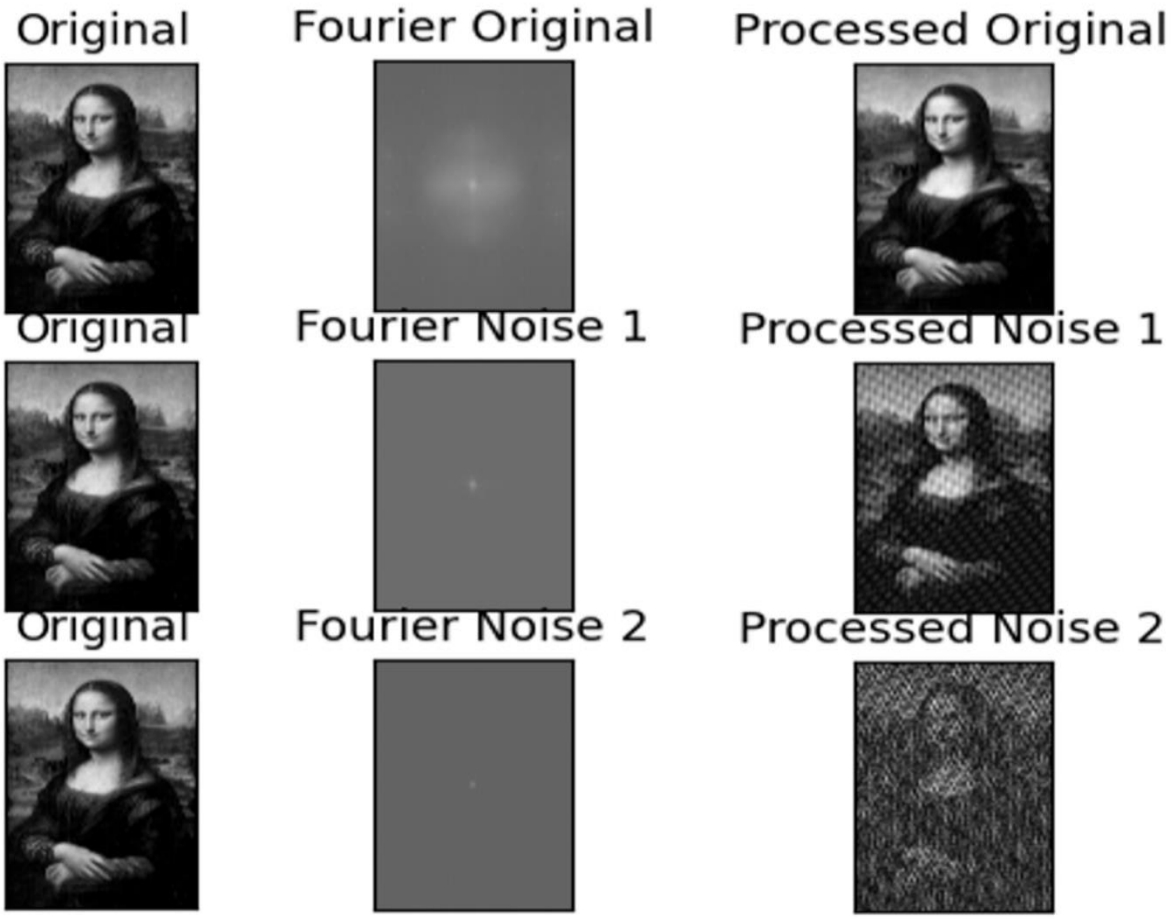

Figure 8: The effects of white noise being implemented in the Fourier domain on the Output image, once the original image has reached this domain, for 3 different noise levels.

Continuing to the noise defect being applied during the Fourier stage, the original images for each of the noise levels should remain identical with only the Fourier and Processed images being notably altered in each case. This is because the noise is only applied during the Fourier stage and its effects carried down the processing line, not up. While the Fourier images for the three noise levels look barely any more hindered than they were for the previous defect, the processed images are considerably more hindered. Notably so is the image for the Processed Noise 2, which

contains the highest dosage of noise applied in the Fourier domain out of the three cases, and in turn leaves the output image almost unrecognisable.

These results strongly show with little doubt that the effect of noise entering the system during the Fourier stage can have a drastic effect on the ability for an image to be recognised. More so than the same magnitude of noise entering before the Fourier stage. In terms of the research question, the detrimental nature of any noise entering during the Fourier stage clearly shows that during the setup of the optical computer, the greatest of care must be taken to remove any possibility of external noise entering the system during the Fourier domain. Failing to do so will result in impediments to the system beyond what would be deemed acceptable for the goal of achieving accurate results. It will inevitably corrupt the output data to the extent it leaves the results nugatory.

3.5. Fringe patterns

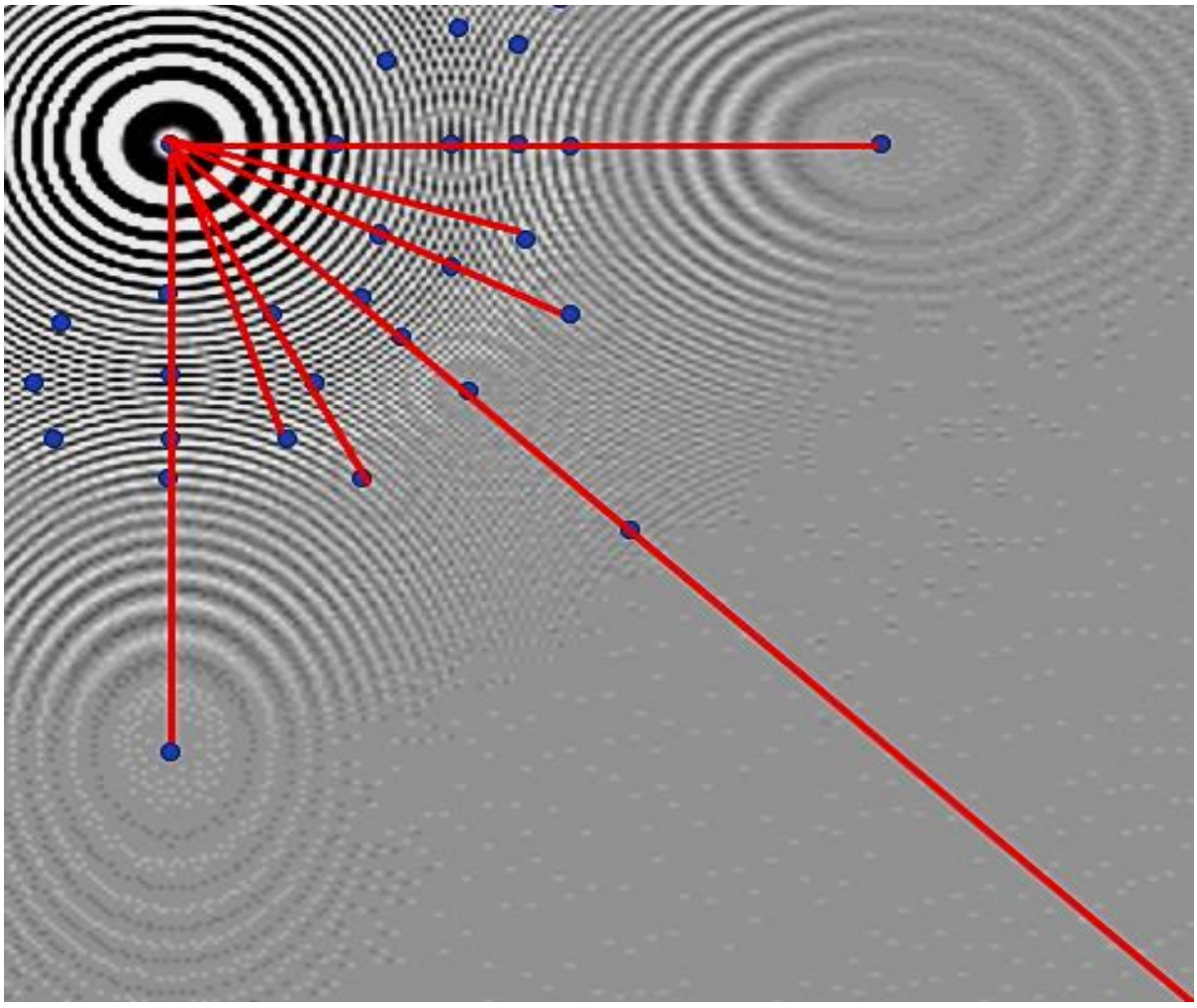

Figure 8: The effects of white noise being implemented in the Fourier domain on the Output image, once the original image has reached this domain, for 3 different noise levels.

The fringe patterns to be analysed here are the patterns which occur surrounding the anticipated diffraction rings. The auxiliary rings produced by the holopy library for the synthetic templates are expected to cause issues when attempting to match against

non-synthetic diffraction patterns from real microbes as they are not supposed to exist at all. What is expected is just a continuation outward of the main (central) diffraction rings. They appear to be separate sets of diffraction rings meaning when they are used as templates, the optical computer is effectively attempting to scan for several sets of diffraction rings in these positions indicated by the blue dots in Fig.9, when it should only be looking for the top-left diffraction pattern which is the main diffraction pattern.

After considerable testing and analysis, it was determined that the auxiliary rings (fringe patterns) being depicted occur along only specific axes denoted by the red lines. However, a reason for their occurrence was yet to be distinguished. Ideas such are mirror boundaries created by holopy at the frame edges were explored to no avail. The checking of the code decerned that the templates being created were in fact displayed correctly, indicating that no numerical error had taken place. Therefore, it was deducted the only possible explanation was down to illusion.

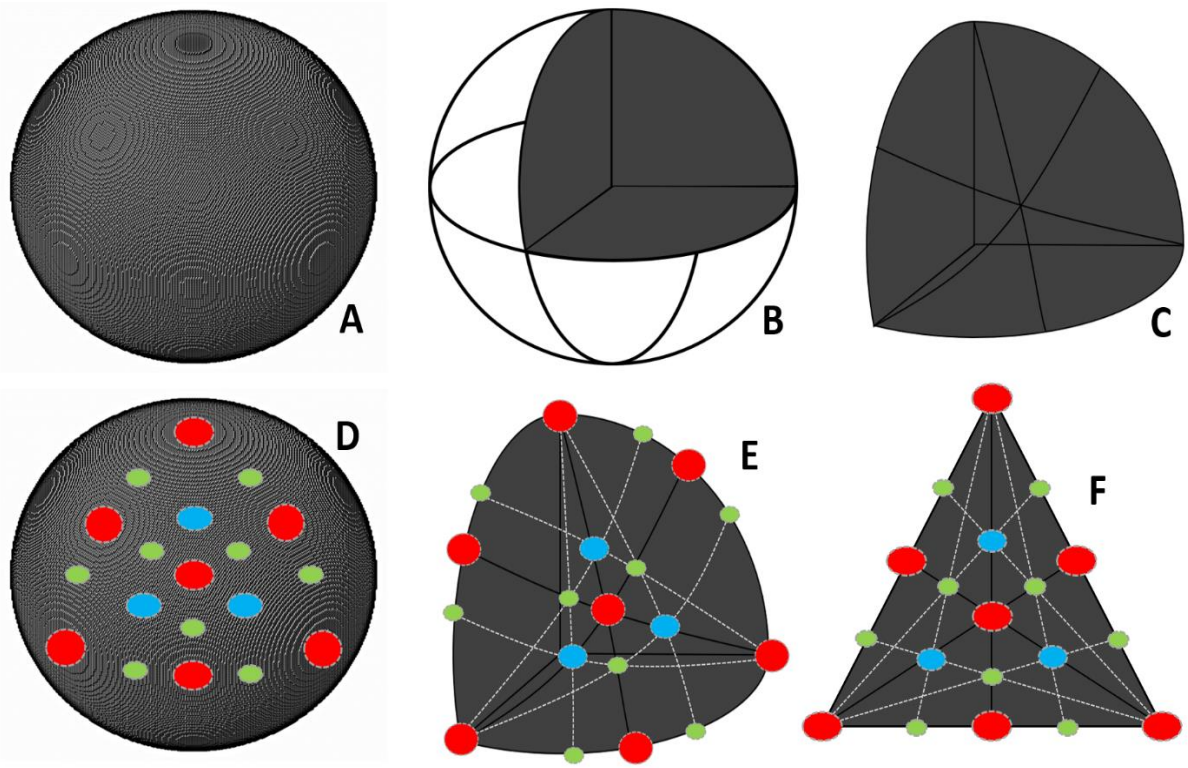

Figure 10: An attempt to explain the fringe patterns by analysis of similar patterns on a cube-formed sphere (A). The sphere is segmented (B), a single segment is focused on (C) and points of interest highlighted (D). Red indicating large ring patterns, blue indicating smaller ring patterns, and green indicating even smaller ring patterns. Taking the single highlighted segment (E) and adjusting the dimensions from 3D to 2D forms a clear indication of positions (F).

In order to explain the illusion, the above images in Fig.10 were formed. It is believed the illusion is formed because of the use of pixelated screens. It is also postulated if infinitesimal pixel sizes were used for monitors, the illusion would in fact not appear. To show this, the idea of finite steps is utilised, and done so by taking a perfect sphere and drawing it in finite cubic steps as seen in A. This plainly forms a very good approximation to a sphere and upon inspection, a recognisable pattern begins to form on the surface akin to that seen in Fig.9. In terms of our fringe pattern, this suggest that taking finite steps (pixel dimensions establishing squares) to form the image in 2D is responsible for the patterns witnessed, and mathematically there is no such pattern

to be witnessed just as when one looks at a perfect sphere (which is in effect a cubic-formed sphere where the cubes are infinitesimal), they do not perceive these patterns either.

To simplify the situation the sphere is segmented in B, which is allowed as each of these segments contains a repeating identical pattern. Lines of interest connecting the largest ring patterns are draw on this segment in C. To clarify which points map to where on the sphere they are highlighted in D. The lines upon which the positions of the ring patterns occur are drawn over the segmented section in E. Finally, the 3D segment is transformed to a 2D plain preserving the lines and points of interest to form the image in F. It is this image which relates to the fringe patterns we perceive in 2D.

While there could be other explanations for the phenomenon, none have been found in related works with little explanation at all ever attempted. Additional analysis should be performed in this area to determine if this thesis is indeed correct as it holds significant implications for the future of image recognition if it happens the rings are in fact not illusions. The image F is drawn to indicate predicted locations of ring patterns correlating to that seen in Fig.9, but further research is required to show why these patterns occur on these overlaps every time the angle between 2 nearby lines is bifurcated forming a new line for occurrence. In terms of the research question, we are to assume the witnessed patterns are indeed illusions caused by pixelated screens and do not actually occur on the templates which are being utilised for matching thus causing no defective attributes.

3.6. THAS3 – Enhancements

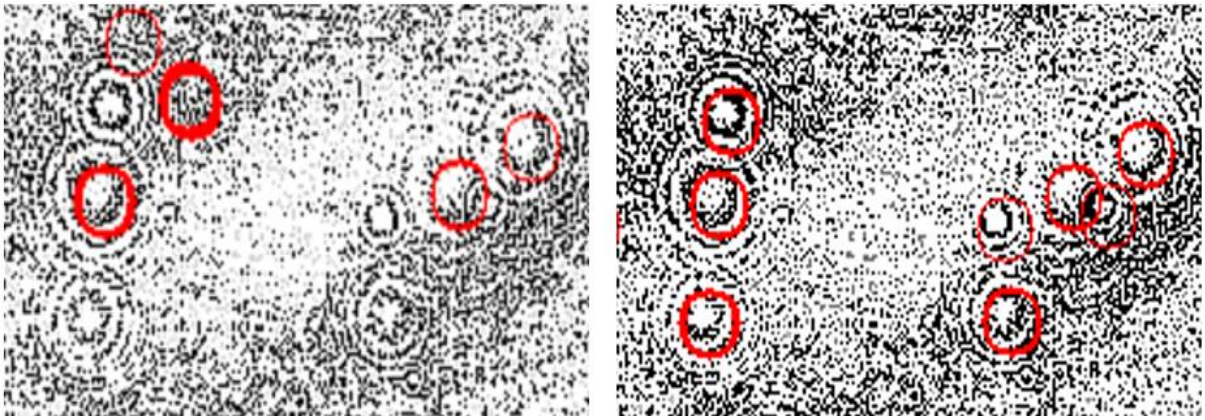

Figure 11: An example of resulting match detections highlighted in red circles for THAS2 on the left and the further developed THAS3 on the right for a frame in the holographic video.

Several adaptions were performed on The Hologram Analysis Systems (THASs) in order to gradually improve several features of the system. Firstly, the accuracy of detections was examined to remove a blurring effect encountered when inspecting the depth dimension (Z) which contained an error of approximately 30 microns in THAS1. It was clear that false detections were being made given this blurring effect and it can be seen in Fig.11 on the left where the detection rings appear thicker as these are multiple detections complied for what is clearly the same archaea. Secondly, the quantity of detections was attempted to be increased such that no usable data was

omitted which would have otherwise contributed to the final results. Again, in the figure on the left several diffraction rings can be seen to not be detected at all, whereas in THAS3 on the right this has been corrected and the previously omitted data has now been detected.

This was achieved with a few key alterations. The template dimensions being used for matching were altered such that the shallower depths which create smaller diffraction rings had reduced template dimensions. This increases the total percentage of diffraction rings on the template, and in turn allowed THAS3 to detect depths which were otherwise omitted or undetected given the lack of features being focused on for those templates.

The template pixel values were altered to create a fading effect as the synthetic templates are 'pure' in that they do not encounter superposition from surrounding templates which they do in the holographic video frames. Therefore, by focusing on the darker centre patches on the original synthetic templates and altering them to a lighter shade, being the average pixel value for the entire template, the effect of superposition was achieved. This in turn means the templates are closer to the actual reality allowing the threshold value to be increased in the matching cases for THAS3, improving accuracy as a whole down to only 10 microns of error.

The holographic video frames were enhanced by THAS3 such that a greater level of contrast (cycles/degree in terms of spatial frequency) was exhibited by the frames before detection began. Along with this, the sharpness of the frames was also increased (where sharpness is determined by the 10-90% rise distance pixel-wise) doing so, the diffraction ring key features were able to be emphasised once again allowing for a higher threshold for matching, decreasing depth error to only 3 microns.

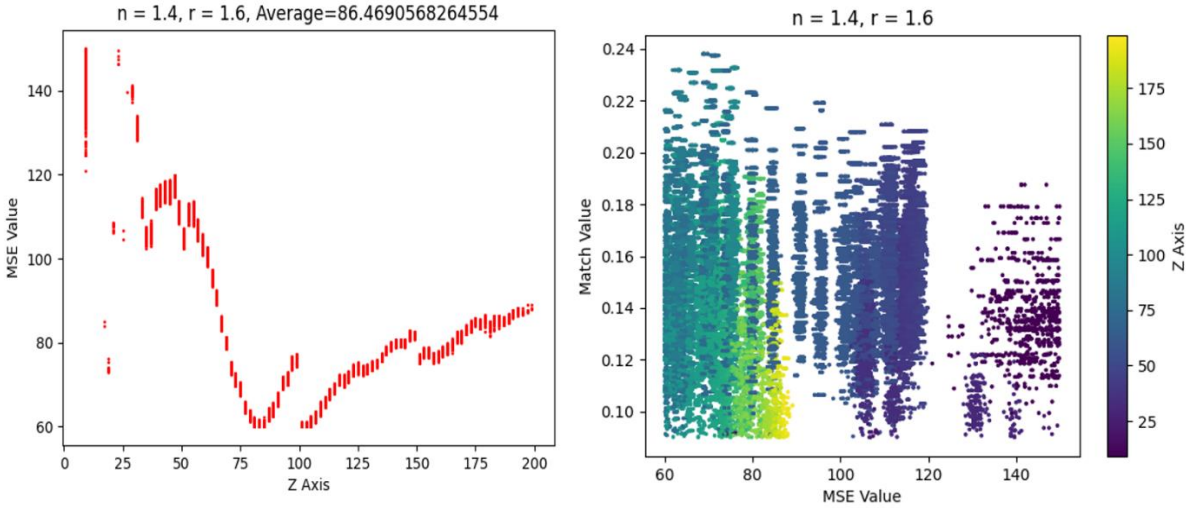

Figure 12: The graphs of MSE against depth (Z), and Match Value (threshold) are shown in the left and right images respectively, with the colour bar denoting depths (Z) for comparison.

Above in Fig.12 are the resulting graphs from THAS3 which use the MSE values for monitoring image matching properties. On the left can be seen the red curved line stutters every 25 microns along the Z axis. This is because of the shading alterations being applied on every set of 25 microns. A better method would be to apply it gradually across the entire Z axis rather than 25-micron groups to remove the stutter.

Overall, the MSE values are kept at an average of 86.5 which comparatively speaking is a little lower than the previous tests. The refractive index and synthetic microbe radius (n and r) were chosen after analysis of various different values due to this particular combination resulting in the highest number of matches. To the right, the graph shows how the matching values achieve a recorded high of 0.24, the highest ever seen was 0.33 and in THAS1 it was as low as 0.04. In terms of the research question, accurate data output has now been achieved consistently along with minimal loss along the processing line.

3.7. THAS3 – Data comparison

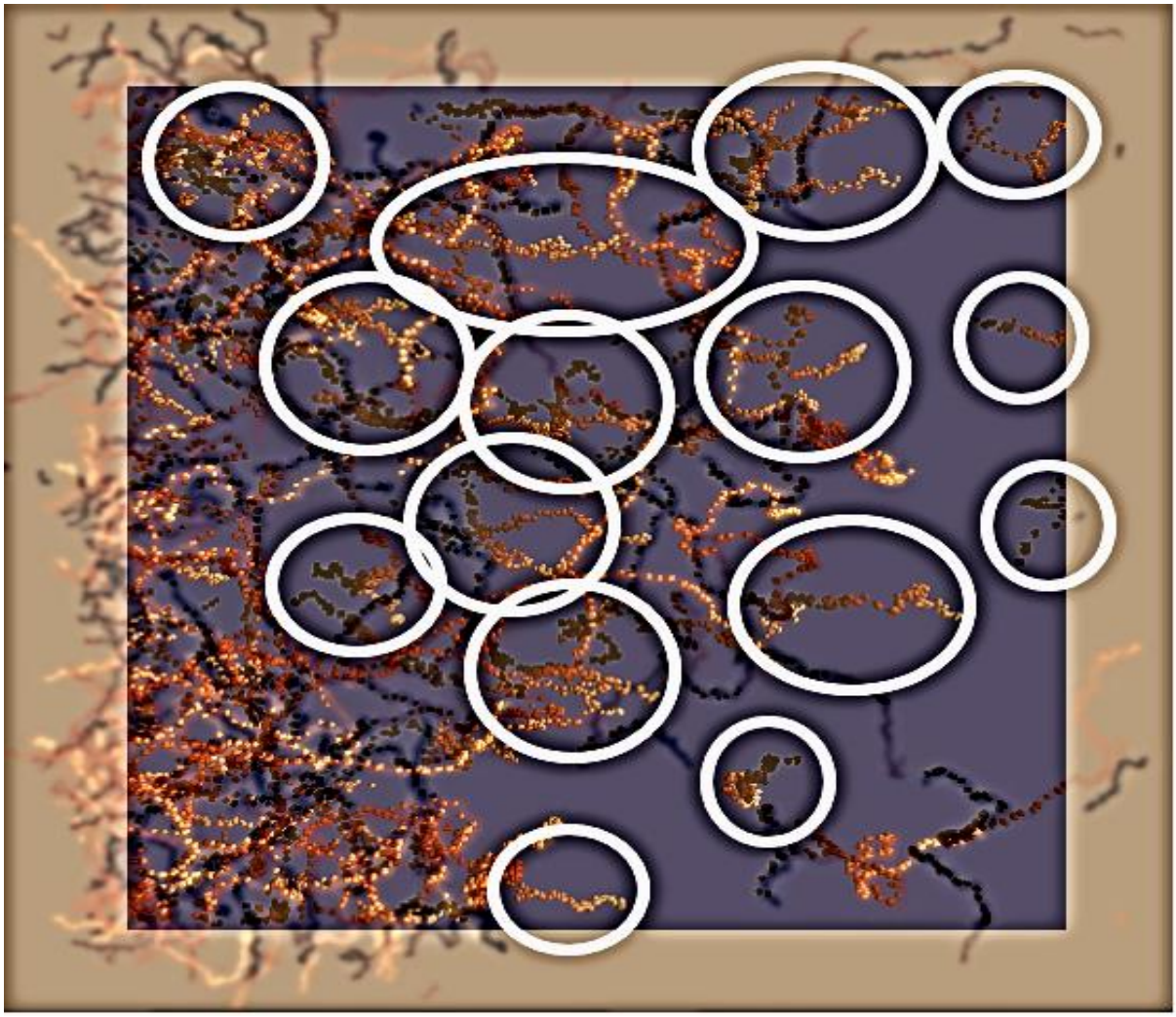

Figure 13: A comparison between THAS3 2D aerial data and an alternative tracking method where THAS3 is overlayed on the alternative which has been faded. Highlighted in white are regions where THAS3 has made considerable detections which were previously not distinguished by the alternative method.

Given the size and number of highlighted white regions in Fig.13 it is evident that THAS3 has drastically increased upon the number of detected paths from the previous alternative method. It should be noted the alternative method incorporates a statistical removal scheme whereby paths are checked for the possibility they are formed by non-living entities moving under Brownian motion and removed from the final plot accordingly to leave only paths of living entities (archaea). However, even with that

additional information, upon further comparison of the data it is seen that several highlighted paths are in fact continuations from paths which the alternative method had detected. Therefore, these are most definitely additional detections made by THAS3 which should have also been made by the alternative method, thus showing the improved ability of THAS3 detections quantity-wise. Regarding the research question, this is completing the objective of minimal data loss along the chain of processing.

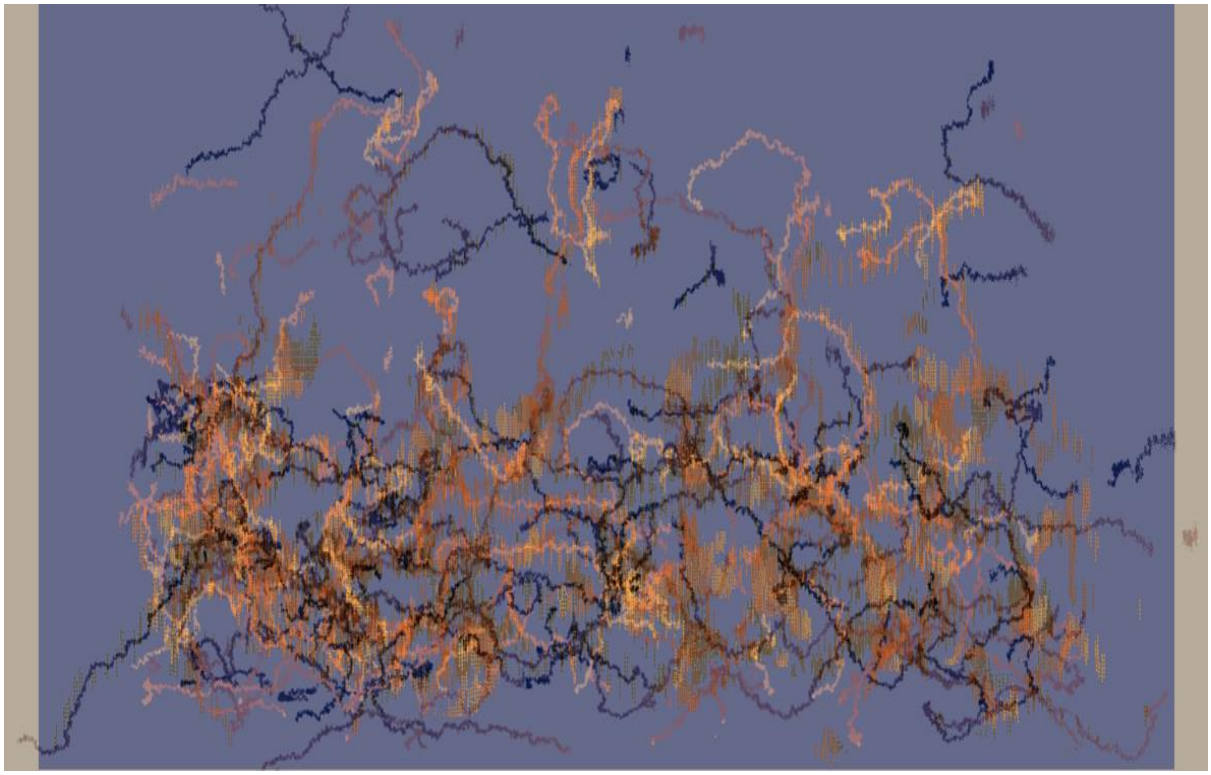

Figure 14: An overlay of THAS3 depth data on an alternative tracking method which has been faded behind.

Continuing to the third dimension of depth comparison seen in Fig.14, it can be seen how there is a complete data overlap between the two sets. The outer boarder in Fig.14 (and Fig.13) which THAS3 does not overlap is due to the method of template matching. While it is difficult to make out, the alternative tracking method has less of an error in the depth position than THAS3 does currently, but it should be mentioned how THAS3's depth error has already been profoundly reduced. The alternative has a depth error of approximately 1 micron compared to THAS3 at 3 microns. While the alternative is superior in this regard, the accuracy already achieved by THAS3 should be adequate for most purposes given the overall lengths of the paths typically tend to be above a hundred microns, resulting in a relative error percentage below 3% for path deviations.

3.8. THAS3 – Operation

In the final stages of development, THAS3 underwent a radical code reform in an attempt to allow the analysis to be digitally performed at highspeed. Simplistically, THAS3 takes a single frame at a time and runs a cross-correlation between that frame and a chosen archive set from the 10,000 synthetic images produced by holopy. While

additional parameters can be set to user preference which impact processing times, a typical processing time for the data seen thus far is 12 minutes. The code reform splits the archive set into multiple segments which run comparisons against the sets of frames in the video independently and recompile the data at the culmination. This is allowed given the CPU usage of THAS3 before the code reform was as low as 22%, and RAM usage was essentially not impacted by the running of THAS3. Therefore, a 4-way split should maximise the CPU usage to just below 100% and in turn, reduce processing times. This was indeed accurate, taking overall processing down to approximately 3 minutes. Taking this idea into the design of the optical computer, the same can be implemented in the setup to allow the system to increase on the already increased processing speeds of the computer.

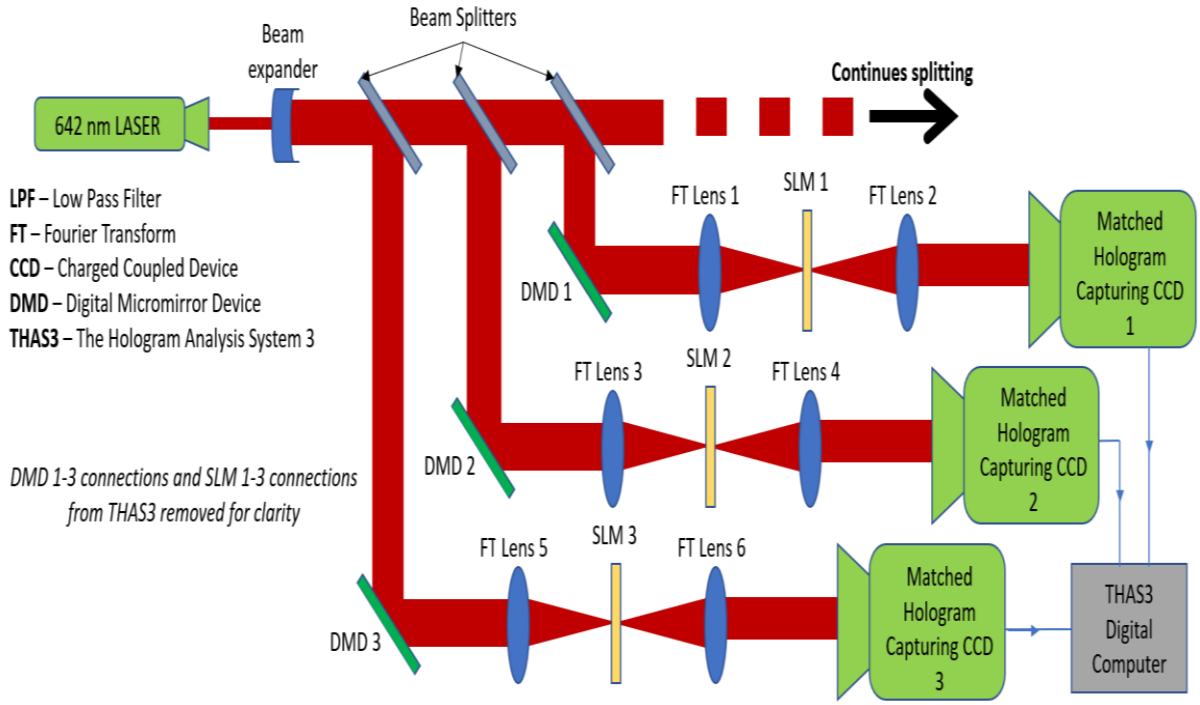

Figure 15: The suggested final design for the optical computer based on all ascertained results. The black arrow indicating possible continuation of splitting is suggesting the repetition of the sections containing a DMD, FT lenses, SLM and CCD as these sections alone are capable of holographic video analysis.

The setup for the proposed optical computer can be seen in Fig.15 where clearly there is a repeated section of the system. The DMDs cast the frames of the holographic video [40] (previously obtained and altered according to the results attained thus far) through the 4F correlator (which is shielded as much as possible against outside noise, again as suggested previously), in which the SLMs produce the templates to be matched against. Each SLM from 1-3 (though can be more) will cast a percentage of the entire archive being matched against simultaneously with the other SLMs to complete the entire archive in a fraction of the time. Upon exiting the 4F correlator and being matched, the output is captured by the CCDs to pinpoint the locations of the templates within the frame and thus the next frame is triggered and the process beings again until all frames of the video have been analysed.

In designing the optical computer this way, the current limitations on SLM refresh rates have been removed. Such that, using more SLMs (as suggested in Fig.15 for

continued splitting) counters the need of faster refreshing in order to maintain pace with the refresh rate of the DMDs, which have less exertions to perform as there is typically a factor of 100 less frames per template to be produced. However, given this splitting of the laser (being the comparatively cheap component in the setup) it could be the case the power is depleted too much having a harmful effect on output of the system despite findings that defects implemented outside of the 4F correlator have little effect on the optical computer output. To correct for this, rather than splitting the laser, several independent lasers could be utilised to ensure power is not depleted.

4. Conclusions

4.1. Deductions drawn.

Noise in the Fourier domain was seen to be the greatest issue when it comes to noise defects in a system. Therefore, the noise in a hologram will have little effect on the overall processing in the computer as this is noise before the Fourier domain. In addition to this, it was found image contrast and sharpness play a significant role in matching a template to the holographic source image. The templates themselves containing the fringe patterns were found to be an illusion and thus have no defective impact on the processing. However, altering darker patches to include the mean background noise can improve the matching of said templates. Deductions can then be made such as better optical systems can now be designed from knowledge of contrast and sharpness impacts. As well as improved archives now being able to be constructed for template matching.

4.2. Objectives accomplished.

The objectives were to identify types of defects possible in the optical system, to test the effects of each defect, and then to attempt to correct for them to produce accurate data with minimal data loss. Three major defect types of Fourier Noise, DMD pixel breakdown, and image noise were distinguished. These were looked at and analysed using SSIM and MSE data to determine their effects on the system. And finally, alterations were made in several stages involving source image parameters (contrast and sharpness) and template details (superposition fading).

New knowledge of how noise implemented in the Fourier stage has a significantly more drastic effect on the process than in any other stage is a success regarding overcoming impediments caused by defects. With this knowledge adaptions to how components are set up can be altered to ensure minimal noise enters the Fourier domain. The analysis of DMD pixel breakdowns now allows the ability to detect a breakdown if one were to occur and therefore be accounted for. Overall, the research question as a whole was successfully answered in depth opening not only new avenues for research but progressing the field another step closer to matching the digital counterpart.

4.3. Future investigations

While The Hologram Analysis System was designed to achieve accurate data outputs with minimal loss, there were areas highlighted which could be further improved in future studies. The CPU for the digital computer was found to work best if there was hyperthreading technology incorporated inside, along with a large number of threads such as the I9-10850K CPU. Further investigations into the accuracy of the depth (Z) axis should be conducted, while 3 microns of error is sufficient for most tracking purposes, for others a higher level of accuracy is required. Methods such as the Gouy phase shift could be examined in addition to the alterations already put forward during the course of this work. Finally, while this report is based on real world data, the construction of the proposed optical computer was never managed. Future studies into the actual construction of the computer and testing in the real world would be useful for classifying other areas previously not assessed for defects or possible enhancements.

5. References

[listed and numbered, in order of appearance in the text]

[1] Wang, C., & Hsu, R. (2017, May). 18-4: Invited Paper: Digital Modulation on Micro Display and Spatial Light Modulator. In *SID Symposium Digest of Technical Papers* (Vol. 48, No. 1, pp. 238-241).

[2] Entwistle, A. (1998). A comparison between the use of a high-resolution CCD camera and 35 mm film for obtaining coloured micrographs. *Journal of microscopy*, *192*(2), 81-89.

[3] Dragulinescu, A., & Cojoc, D. (2005, December). Optical correlators: systems and domains of applications. In *Advanced Topics in Optoelectronics, Microelectronics, and Nanotechnologies II* (Vol. 5972, p. 59721F). International Society for Optics and Photonics.

[4] Stark, H. (Ed.). (2012). *Application of Optical Fourier Transforms*. Elsevier.

[5] Pedersen, M. M., Smedegaard, J., Jensen, P. K., Heegaard, S., Jensen, O. A., & Prause, J. U. (2005). A comparison of colour micrographs obtained with a charged couple device (CCD) camera and a 35-mm camera. *Acta Ophthalmologica Scandinavica*, *83*(1), 89-93.

[6] Dudley, D., Duncan, W. M., & Slaughter, J. (2003, January). Emerging digital micromirror device (DMD) applications. In *MOEMS display and imaging systems* (Vol. 4985, pp. 14-25). International Society for Optics and Photonics.

[7] Yezhov, P. V., & Kuzmenko, A. V. (2004, June). Synthesized phase objects instead of real ones for optical-digital recognition systems. In *Sixth International Conference on Correlation Optics* (Vol. 5477, pp. 412-421). International Society for Optics and Photonics.

[8] Chan, W. L., Chen, H. T., Taylor, A. J., Brener, I., Cich, M. J., & Mittleman, D. M. (2009). A spatial light modulator for terahertz beams. *Applied Physics Letters*, *94*(21), 213511.

[9] Steward, E. G., & Hecht, E. (1986). Fourier Optics: An Introduction.

[10] Bracewell, R. N., & Bracewell, R. N. (1986). *The Fourier transform and its applications* (Vol. 31999, pp. 267-272). New York: McGraw-Hill.

[11] García-Martínez, P., Marco, D., Martínez-Fuentes, J. L., del Mar Sánchez-López, M., & Moreno, I. (2020). Efficient on-axis SLM engineering of optical vector modes. *Optics and Lasers in Engineering*, *125*, 105859.

[12] Li, S. Q., Xu, X., Veetil, R. M., Valuckas, V., Paniagua-Domínguez, R., & Kuznetsov, A. I. (2019). Phase-only transmissive spatial light modulator based on tunable dielectric metasurface. *Science*, *364*(6445), 1087-1090.

[13] Wang, Z., Bovik, A. C., Sheikh, H. R., & Simoncelli, E. P. (2004). Image quality assessment: from error visibility to structural similarity. *IEEE transactions on image processing*, *13*(4), 600-612.

[14] Wang, Z. (2003). The SSIM index for image quality assessment. *https://ece. uwaterloo. ca/~ z70wang/research/ssim*.

[15] Wang, Z., & Bovik, A. C. (2002). A universal image quality index. *IEEE signal processing letters*, *9*(3), 81-84.

[16] Tomasi, C. (2020). Image Correlation, Convolution and Filtering.

[17] Palubinskas, G. (2017). Image similarity/distance measures: what is really behind MSE and SSIM?. *International Journal of Image and Data Fusion*, *8*(1), 32-53.

[18] Tyson, R. K. (2014). *Principles and Applications of Fourier Optics*. IOP Publishing, Bristol, UK.

[19] Brunet, D., Vrscay, E. R., & Wang, Z. (2011). On the mathematical properties of the structural similarity index. *IEEE Transactions on Image Processing*, *21*(4), 1488-1499.

[20] Grogan, S. P., Chung, P. H., Soman, P., Chen, P., Lotz, M. K., Chen, S., & D'Lima, D. D. (2013). Digital micromirror device projection printing system for meniscus tissue engineering. *Acta biomaterialia*, *9*(7), 7218-7226.

[21] Garcia-Sucerquia, J., Xu, W., Jericho, M. H., & Kreuzer, H. J. (2006). Immersion digital in-line holographic microscopy. *Optics letters*, *31*(9), 1211-1213.

[22] Voelz, D. (2011). Computational fourier optics: a MATLAB tutorial. Society of Photo-Optical Instrumentation Engineers.

[23] Ahmed, N. (1985). FAST TRANSFORMS, algorithms, analysis, applications. *Proceedings of the IEEE*, *73*(3), 494-494.

[24] Duffieux, P. M. (1983). The Fourier transform and its applications to optics. *The Fourier Transform 2nd Edition and Its Applications to Optics by PM Duffieux New York*.

[25] Keane, R. D., & Adrian, R. J. (1992). Theory of cross-correlation analysis of PIV images. *Applied scientific research*, *49*(3), 191-215.

[26] Wang, Z., Bovik, A. C., & Lu, L. (2002, May). Why is image quality assessment so difficult?. In *2002 IEEE International Conference on Acoustics, Speech, and Signal Processing* (Vol. 4, pp. IV-3313). IEEE.

[27] Reichenbach, M., Seidler, R., Pfundt, B., & Fey, D. (2014). Fast image processing for optical metrology utilizing heterogeneous computer architectures. *Computers & Electrical Engineering*, *40*(4), 1158-1170.

[28] Eskicioglu, A. M., & Fisher, P. S. (1995). Image quality measures and their performance. *IEEE Transactions on communications*, *43*(12), 2959-2965.

[29] Chen, M. J., & Bovik, A. C. (2011). Fast structural similarity index algorithm. *Journal of Real-Time Image Processing*, *6*(4), 281-287.

[30] Silverstein, D. A., & Farrell, J. E. (1996, September). The relationship between image fidelity and image quality. In *Proceedings of 3rd IEEE International Conference on Image Processing* (Vol. 1, pp. 881-884). IEEE.

[31] Girod, B. (1993). What is wrong with mean-squared error?. *Digital images and human vision*, 207-220.

[32] Wang, Z., & Bovik, A. C. (2009). Mean squared error: Love it or leave it? A new look at signal fidelity measures. *IEEE signal processing magazine*, *26*(1), 98-117.

[33] Ramachandran, P., & Varoquaux, G. (2011). Mayavi: 3D visualization of scientific data. *Computing in Science & Engineering*, *13*(2), 40-51.

[34] Bradski, G., & Kaehler, A. (2008). *Learning OpenCV: Computer vision with the OpenCV library*. " O'Reilly Media, Inc.".

[35] Barkley, S., Dimiduk, T. G., Fung, J., Kaz, D. M., Manoharan, V. N., McGorty, R., ... & Wang, A. (2019). Holographic microscopy with Python and HoloPy. *Computing in Science & Engineering*, *22*(5), 72-82.

[36] Siahaan, V., & Sianipar, R. H. (2019). *LEARNING PyQt5: A Step by Step Tutorial to Develop MySQL-Based Applications*. SPARTA PUBLISHING.

[37] Dosselmann, R., & Yang, X. D. (2011). A comprehensive assessment of the structural similarity index. *Signal, Image and Video Processing*, *5*(1), 81-91.

[38] Zlokazov, E. Y. (2020). Methods and algorithms for computer synthesis of holographic elements to obtain a complex impulse response of optical information processing systems based on modern spatial light modulators. *Quantum Electronics*, *50*(7), 643.

[39] Schroeder, M. R. (1981). Modulation transfer functions: Definition and measurement. *Acta Acustica united with Acustica*, *49*(3), 179-182.

[40] Pearson, D. E. (1995). Developments in model-based video coding. *Proceedings of the IEEE*, *83*(6), 892-906.

Acknowledgements

I would like to thank Dr Laurence Wilson from the University of York for his dedicated input throughout the course of this project. Not only for his invaluable experience in the field but also the suppling of the holographic data which was used on countless occasions during the testing of The Hologram Analysis Systems 1-3.

I would also like to thank Mr Alexis Ridler from BAE Systems for his input during the project in terms of logical methods of producing the final THAS3 application, as well as providing useful feedback on project presentations delivered by myself.